PROCEEDINGS OF SCIENCE

The Radio Detector of the Pierre Auger Observatory

Jörg R. Hörandel[a,b,*] **and the Pierre Auger Collaboration**[c]

[a] *Radboud University, Department of Astrophysics/IMAPP, P.O. Box 9010, 6500 GL Nijmegen, The Netherlands*

[b] *Vrije Universiteit Brussel, Pleinlaan 2, 1050 Brussels, Belgium*

[c] *Av. San Martin Norte 304, Malargüe, Mendoza, Argentina*

E-mail: j.horandel@astro.ru.nl

To measure the properties of the highest-energy particles in the Universe with unprecedented precision, we have upgraded the Pierre Auger Observatory. A crucial component of this upgrade is the Radio Detector. Radio antennas have been added to all 1660 positions of the surface detector array, covering an area of 3000 km^2. The antennas detect radio emission, emitted by extensive air showers in the frequency band from 30 to 80 MHz in two polarization directions - one parallel and one perpendicular to the Earth magnetic field. For inclined air showers with zenith angles above 60 degrees, the radio antennas provide a clean measurement of the electromagnetic shower component, while the water-Čerenkov detectors measure the muonic component. Large-scale deployment in the Argentinian Pampa Amarilla started around June 2023 and has been completed in 2024. The deployment is accompanied by extensive calibration efforts both, in the laboratory and in the field. The signal chain is characterized in the laboratory. Galactic radio emission is used as a reference signal and the antenna patterns are verified through in-situ calibrations with a reference antenna. Commissioning of the system is in full progress as well as the analysis of first measured air showers. We present first air showers measured with the largest radio detector for cosmic rays in the world.

7th International Symposium on Ultra High Energy Cosmic Rays (UHECR2024)
17-21 November 2024
Malargüe, Mendoza, Argentina

[*] Speaker

PoS(UHECR2024)094

1. Introduction

Nature provides particles at enormous energies, exceeding 10^{20} eV – orders of magnitude beyond the capabilities of human-made facilities like the Large Hadron Collider at CERN. At the highest energies, the precise particle types are not yet known, they might be ionised atomic nuclei or even neutrinos or photons. Even for heavy nuclei (e.g. iron nuclei) their Lorentz factors $\gamma = E_{tot}/mc^2$ exceed values of $\gamma > 10^9$. The existence of such particles arises immediate, yet unanswered questions: • What are the physics processes involved to produce these particles? • Are they decay or annihilation products of Dark Matter[1, 2]? If they are accelerated in violent astrophysical environments: • How is Nature able to accelerate particles to such energies? • What are the sources of these particles? Do we understand the physics of these sources? • Is their origin connected to the recently observed mergers of compact objects – gravitational wave sources [3–8]? These highly-relativistic particles also provide the unique possibility to study particle physics at its extremes: • Is Lorentz invariance (still) valid under such conditions [9–14]? • How do these particles interact? • Are their interactions described by the Standard Model of particle physics? When these energetic particles interact with the atmosphere of the Earth, hadronic interactions can be studied in the extreme kinematic forward region (with pseudorapidities $\eta > 15$) [15].

2. Radio Detection of extensive air showers

The radio emission in extensive air showers (EASs) originates from different processes (see Fig. 1 for an illustration). The dominant mechanism is of geomagnetic origin [16–18]: electrons and positrons in the shower are accelerated in opposite directions by the Lorentz force exerted by the magnetic field of the Earth. The generated radio emission is linearly polarised in the direction of the Lorentz force ($v \times B$), where v is the propagation velocity vector of the shower (parallel to the shower axis) and B represents the direction and strength of the Earth magnetic field. A secondary contribution to the radio emission arises from the excess of electrons at the front of the shower (Askaryan effect) [19]. This excess builds up from electrons that are knocked out of atmospheric molecules by interactions with shower particles, while positrons are depleted through annihilation. This charge excess contribution is radially polarised, pointing towards the shower axis. The resulting emission measured at the ground is the sum of both components. Interference between these components may be constructive or destructive, depending on the position of the observer/antenna relative to the shower. The emission is strongly beamed in the forward direction due to the relativistic velocities of the particles. Additionally, the emission propagates through the

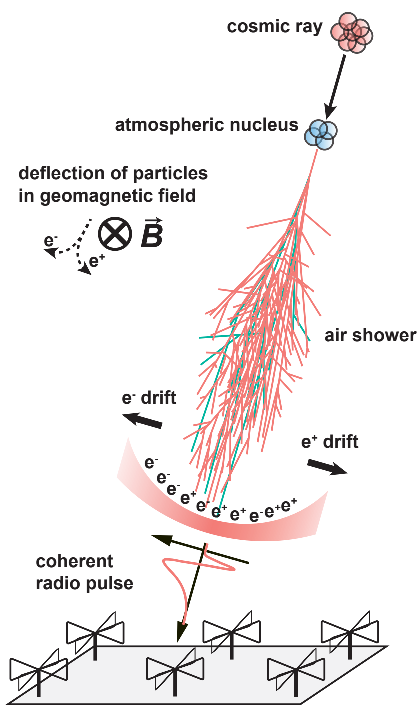

Figure 1: Schematic view of an extensive air shower.

atmosphere, which has a non-unity index of refraction that changes with altitude. This leads to relativistic time-compression effects, most notably producing a ring of amplified emission around the Čerenkov angle [20]. By precisely measuring the polarisation direction of the electric field at various positions within the air shower footprint, the relative contribution of the main emission processes has been measured [21, 22].

Horizontal air showers (HAS, see Fig. 2) [23] with zenith angles $\Theta > 60^\circ$ traverse a big amount of atmosphere until they are detected. The thickness of the atmosphere in horizontal direction amounts to about 40 times the column density of the vertical atmosphere. Thus, the e/m shower component is mostly absorbed and only muons are detected with the water-Čerenkov detectors of the Surface Detector. The atmosphere is transparent for radio emission in our band $(30 - 80$ MHz) and radio measurements are an ideal tool for a calorimetric measurement of the e/m component in HAS.

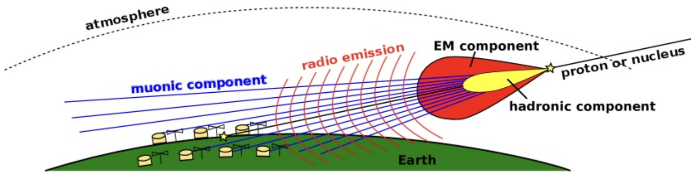

Figure 2: Illustration of a horizontal air shower.

3. The Radio Detector and the upgraded Pierre Auger Observatory

Recently, the Pierre Auger Observatory has been upgraded to improve its sensitivity to identify the type incoming particle (mass sensitivity) [24]. The deployment of all components is almost completed and commissioning is ongoing, preparing to take data for the coming decade. A Scintillator Surface Detector (SSD) has been installed on top of each water-Čerenkov Detector (WCD) [25]. Scintillator bars with an area of 2 m^2 are enclosed in an aluminium box and read out by a PMT via wavelength shifting fibres. The electronics of the Surface Detector (SD) has been upgraded [26]: the newly developed Upgraded Unified Board (UUB) features a 12-bit ADC with 120 MHz sampling rate to read out the PMTs of the WCD and the SSD. All data are send via the existing communication system to a central Data Acquisition System (DAQ).

The **Radio Detector (RD)**: Two aluminium rings, forming the dual-polarised antenna, are mounted on a fibreglass mast on top of each WCD (see Fig. 3, left) [27, 28]. One of the antenna rings is aligned parallel to the orientation of the Earth's magnetic field, while the second one is perpendicular to it. The antenna is a Short Aperiodic Loaded Loop Antenna (SALLA) [29]. With its diameter of 122 cm, it is tailored to the frequency range of interest of 30 to 80 MHz, for which it delivers a virtually uniform response with very little dispersion. The antenna arms are held in place by injection-moulded plastic housings, which also contain the pre-amplifier at the top, and the load resistor at the bottom. The antenna features a 392 Ω resistor at the bottom, which shapes the main lobe towards the zenith and, at the same time, suppresses dependence on structures below the antenna, in particular the SSD, the WCD, and potentially variable ground conditions. Each of the two antenna channels is read out by a 12-bit ADC with a sampling rate of 250 MHz. Before digitisation, the signals are amplified by a total of 36 dB and filtered by a band-pass filter in the range 30 to 80 MHz. A Field Programmable Gate Array (FPGA) coordinates data exchange with the UUB, which requests radio data whenever a trigger is received from the WCD. On the UUB

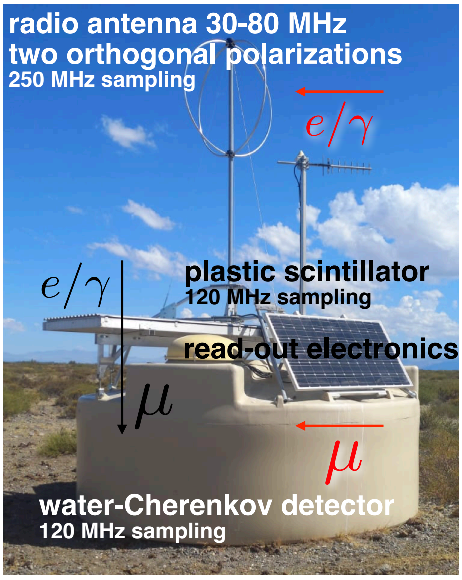

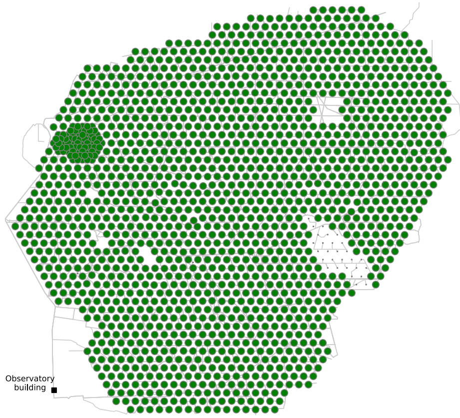

Figure 3: Left: a station of the surface detector array of the Pierre Auger Observatory. Right: deployment status of the Radio Detector, basically all positions are operational, forming a 3000 km^2 radio detector array.

the RD data are included in the standard data stream. All SD positions have been equipped with radio antennas, enabling radio detection on different grid sizes of 1500 m, 750 m, and 433 m (see Fig. 3, right). Covering a total area of 3000 km^2 the Radio Detector is the largest radio detector for (charged) cosmic rays, neutrinos, and gamma rays, orders of magnitude larger than all other rexisting facilities [30]. The main objective is the detection of inclined air showers with zenith angles $\theta > 60^\circ$ with the 1500 m grid. The grids with shorter distances will be used to perform radio detection of vertical showers (with $\theta < 60^\circ$). Of particular interest (to study hadronic interactions) will be air showers recorded simultaneously with the RD and the Underground Muon Detector [31], allowing for a direct, simultaneous measurement of the electromagnetic (e/m) and muonic shower components.

The Radio Detector adds unique physics capabilities to the Pirre Auger Observatory [32]. We expect to measure about 3000 to 4000 cosmic rays with energies $> 10^{19}$ eV in the next decade. The goal of the upgraded Observatory is to exploit separate measurements of the e/m and muonic content of air showers to determine the mass of the incoming cosmic rays. While for vertical air showers the separate measurement of the two components is achieved by the combination of the WCD and the SSD, for inclined air showers (with zenith angle $\Theta > 60^\circ$) the combination of the RD and WCD is used. The RD delivers an accurate measurement of the e/m energy of an air shower, while the WCD measures the virtually pure muon content of inclined air showers. The combination thus allows us to study the muon content of extensive air showers, as has previously been performed using the combination of WCD and Fluorescence Detector data [33], yet with orders of magnitude lower statistics than will be possible with the RD.

4. End-to-end calibration of the signal chain

The active components of the RD electronics, the low-noise amplifiers (LNAs) and the digitisers have been thermally cycled to simulate ageing and take care of eventual changes in performance as a function of time. All units have been end-to-end calibrated in the laboratory, recording parameters like gain and phase shifts as a function of frequency. The antenna pattern of the Short Aperiodic Loaded Loop Antenna (SALLA) [29] has been simulated with the NEC software. The antenna pattern has been verified through in-situ measurements (see e.g. [34]) in the field with a drone, carrying a reference antenna in a defined pattern above a RD station. The diffuse Galactic radio emission is well measured [35], this is used as a standard reference signal to calibrate the RD in-situ [36]. The galactic radio emission is recorded periodically on each station locally and is used to correct for potential time-dependent changes in the parameters. It should be noted that the absolute calibration of the full electronics chain (performed in the laboratory) agrees within 5% uncertainty with the parameters obtained from the Galactic emission [37]. This demonstrates our excellent understanding of the complete signal chain. The atmospheric electric fields are continuously monitored at 5 positions in the SD array. This allows to generate a veto against strong atmospheric electric field during thunderstorms [38], which would distort the energy measurements of a shower. This yields absolutely calibrated time traces for each antenna and polarisation direction. The calibration chain is illustrated in Fig. 4. A study with an engineering array (AERA) demonstrates the long-term stability of the radio detection technique [39]. Only marginal deviations, compatible with zero have been found over a period of nearly 10 years.

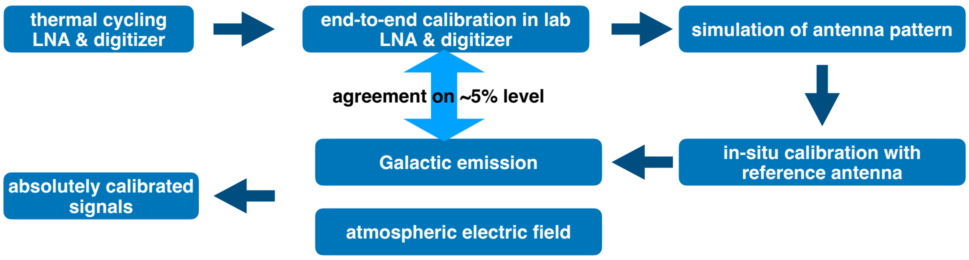

Figure 4: Calibration concept of the RD, see text.

5. First data

At the time of writing, installation has been completed and commissioning of the RD systems is ongoing. First RD data are being analysed in parallel with the already commissioned parts of the array. The first data coming in look very promising. For illustration, in Fig. 5, a measured air shower is shown with an energy of almost 4×10^{19} eV, coming in just 5° above the horizon. The energy fluence as a function of distance to the shower axis has been fitted with a specially adapted function for HAS [40]. This function describes the data very well and yields the total e/m energy delivered to the ground in the form of radio waves (in the $30 - 80$ MHz band). The shower has been reconstructed independently, using the information from the RDs and the WCDs.

Both, the direction (azimuth and zenith angles) as well as the energy agree perfectly within their uncertainties. The location of the shower axis, intersecting with the ground, is slightly offset between the particle content of the shower (WCD) and the radiation (RD), this is caused by refractive effects during the propagation of the radio waves in the atmosphere [41]. For illustration and to facilitate cross checks an independent reconstruction has been applied for Fig. 5. The goal of future work is to establish a hybrid reconstruction, combining the information from the RDs and WCDs.

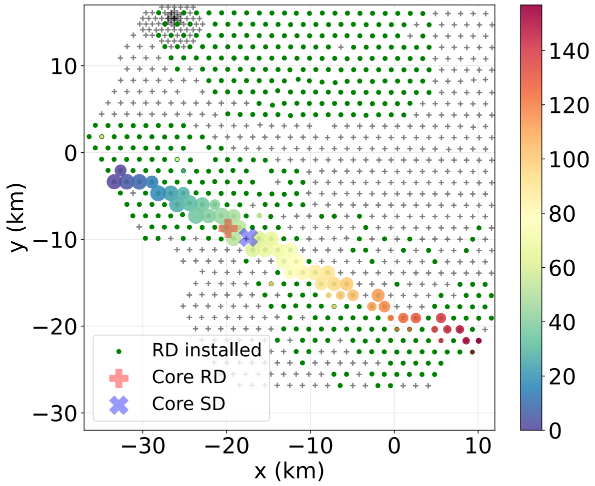

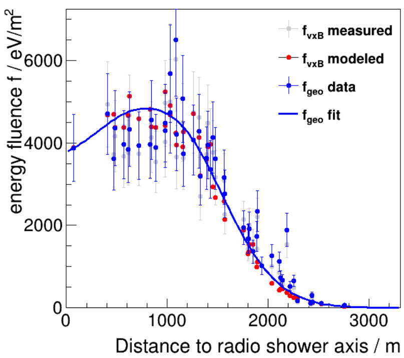

	RD	SD
Azimuth (deg)	157.0±0.1	157.0±0.1
Zenith (deg)	84.7±0.1	84.7±0.1
Energy (EeV)	36.23 ± 3.34	38.55 ± 2.92
Core X (km)	-19.80 ±0.90	-17.40±0.88
Core Y (km)	-8.73 ±0.90	-9.78±0.45

Figure 5: An air shower measured with the RD. Left: footprint of the shower, the colored circles represent measured (geomagnetic) radio energy fluence. Right: energy fluence as a function of distance to the shower core with a fit, see text. For illustration, the shower has been reconstructed independently with the water-Čerenkov detectors (SD) and the radio antennas (RD).

Another data-driven approach to verify the performance of the RD system is to investigate the measured e/m energy (obtained by the RD) as a function of the total shower energy, derived from the WCD measurements, as illustrated in Fig. 6. This is a very important plot since it illustrates the end-to-end verification of the complete signal chain. The absolute energy scale obtained by the RD is fully compatible with the well established energy scale of the WCD. It should be noted that the data shown were taken during the installation, i.e. only with a fraction of the full 3000 km^2 array. Therefore, only loose quality cuts have been applied (to keep some showers for the analysis), which results in a larger scattering of points around the main diagonal. In the future, when we can apply stricter quality cuts, we expect a much narrower distribution along the main diagonal. It should also be noted that the e/m energy is always expected to be slightly smaller than the total shower energy. The difference is caused by energy carried away in the shower by neutrinos and high-energy muons, i.e., the "missing energy".

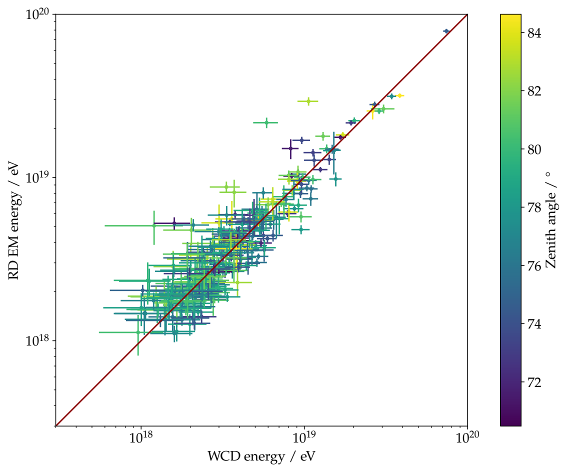

Figure 6: Measured e/m energy (from the RD) in showers as a function of total CR energy, derived from WCD measurements.

6. Outlook

On 16 November 2024 the *International Agreement* to operate the Pierre Auger Observatory was extended until 2035. We are looking forward to the next decade in which we expect new results, that will provide us new insights to the understanding of physics processes under extreme conditions and the origin of the highest-energy particles in the Universe.

References

[1] E. Alcantara, L. A. Anchordoqui, and J. F. Soriano *Phys. Rev. D* **99** (2019) 103016.

[2] R. Aloisio, S. Matarrese, and A. V. Olinto *JCAP* **08** (2015) 024.

[3] P. Lipari, "Cosmic Rays, Gamma rays, Neutrinos and Gravitational Waves," in *11th Workshop on Science with the New generation of High Energy Gamma-ray Experiments (SciNeGHE 2016) Pisa, Italy, October 18-21, 2016*. 2017. `arXiv:1707.02732 [astro-ph.HE]`. `https://inspirehep.net/record/1609211/files/arXiv:1707.02732.pdf`.

[4] M. Branchesi *J. Phys. Conf. Ser.* **718** (2016) 022004.

[5] L. A. Gergely and P. L. Biermann *Astrophys. J.* **697** (2009) 1621–1633.

[6] L. A. Gergely and P. L. Biermann *J. Phys. Conf. Ser.* **122** (2008) 012040.

[7] L. A. Gergely, P. L. Biermann, and L. I. Caramete *Class. Quant. Grav.* **27** (2010) 194009.

[8] M. Tápai, L. A. Gergely, Z. Keresztes, P. J. Wiita, Gopal-Krishna, and P. L. Biermann *Astron. Nachr.* **334** (2013) 1032.

[9] F. R. Klinkhamer and M. Risse *Phys. Rev. D* **77** (2008) 117901.

[10] F. R. Klinkhamer, M. Niechciol, and M. Risse *Phys. Rev. D* **96** (2017) 116011.

[11] R. Aloisio, P. Blasi, P. L. Ghia, and A. F. Grillo *Phys. Rev. D* **62** (2000) 053010.

[12] R. Cowsik, T. Madziwa-Nussinov, S. Nussinov, and U. Sarkar *Phys. Rev. D* **86** (2012) 045024.

[13] H. Martínez-Huerta and A. Pérez-Lorenzana *Phys. Rev. D* **95** (2017) 063001.

[14] R. G. Lang, [Pierre Auger Collab.] *PoS* **ICRC2019** (2020) 327.

[15] P. Abreu *et al.*, [Pierre Auger Collab.] *Phys. Rev. Lett.* **109** (2012) 062002.

[16] F. Kahn and I. Lerche *Royal Society of London Proceedings Series A* **289** (1966) 206.

[17] H. Allan, *Progress in Elementary Particles and Cosmic Ray Physics*, p. 169. J.G. Wilson and S.G. Wouthuysen eds., North Holland, 1971.

[18] D. Ardouin *et al.* *Astropart. Phys.* **31** (2009) 192–200.

[19] G. Askaryan *Journal of the Physical Society of Japan Supplement* **17** (1962) C257.

[20] A. Nelles, P. Schellart, S. Buitink, A. Corstanje, K. de Vries, *et al.* *Astropart.Phys.* **65** (2014) 11–21.

[21] P. Schellart, S. Buitink, A. Corstanje, J. Enriquez, H. Falcke, *et al.* *JCAP* **1410** (2014) 014.

[22] A. Aab *et al.*, [Pierre Auger Collaboration Collab.] *Phys.Rev.* **D89** (2014) 052002.

[23] A. Aab *et al.*, [Pierre Auger Collab.] *JCAP* **1810** (2018) 026.

[24] A. Castellina, [Pierre Auger Collab.] *EPJ Web Conf.* **210** (2019) 06002.

[25] G. Cataldi, [Pierre Auger Collab.] *PoS* **ICRC2021** (2021) 251.

[26] A. Abdul Halim *et al.*, [Pierre Auger Collab.] *JINST* **18** (2023) P10016.

[27] J. R. Hörandel, [Pierre Auger Collab.] *EPJ Web Conf.* **210** (2019) 06005.

[28] J. R. Hörandel, [Pierre Auger Collab.] *EPJ Web Conf.* **216** (2019) 01010.

[29] O. Krömer *et al.*, [Pierre Auger Collab.] *Proceedings of the 31st ICRC, Lodz, Poland* **ICRC2009** (2009) 1232.

[30] T. Huege *Phys. Rept.* **620** (2016) 1–52.

[31] A. Abdul Halim *et al.*, [Pierre Auger Collab.] *PoS* **ICRC2023** (2023) 267.

[32] T. Huege, [Pierre Auger Collab.] *EPJ Web Conf.* **283** (2023) 06002.

[33] A. Aab *et al.*, [Pierre Auger Collab.] *Phys. Rev. Lett.* **126** (2021) 152002.

[34] A. Aab *et al.*, [Pierre Auger Collab.] *JINST* **12** (2017) T10005.

[35] M. Büsken, T. Fodran, and T. Huege *Astron. Astrophys.* **679** (2023) A50.

[36] P. Abreu *et al.*, [Pierre Auger Collab.] *PoS* **ICRC2021** (2021) 270.

[37] T. Fodran, [Pierre Auger Collab.] *PoS* **ARENA2022** (2023) 043.

[38] P. Schellart, T. Trinh, S. Buitink, A. Corstanje, J. Enriquez, *et al.* *Phys.Rev.Lett.* **114** (2015) 165001.

[39] R. de Almeida *et al.*, [Pierre Auger Collab.] *PoS* **ICRC2023** (2023) 279.

[40] F. Schlüter and T. Huege *JCAP* **01** (2023) 008.

[41] F. Schlüter, M. Gottowik, T. Huege, and J. Rautenberg *Eur. Phys. J. C* **80** (2020) 643.